RESEARCH   **Open Access**

Influence of the topographic effect on the seismic response of buried pipelines

Jahangir Elyasi[1], Morteza Bastami[2*] , Mohsen Kamalian[2] and Mehdi Derakhshandi[1]

Abstract

Detailed study of the response of pipelines during seismic excitation can help reduce physical and financial losses during and after an earthquake. The current research investigated the seismic behavior of pipelines passing through variations in topography using two-dimensional and three-dimensional modeling. Their behavior has been modeled at the crest and toe of a slope and during longitudinal passage through the topography. The effects of the soil stiffness, diameter-to-thickness ratio of the pipeline, height-to-half-width ratio (shape factor), and input wave characteristics on the performance of the pipeline have been investigated. The results indicate that topographic effects can increase the strain on pipelines and the factors studied are crucial to accommodating this potential hazard.

Keywords: Earthquake, Pipeline, Topographic effect

Introduction

Buried pipelines are lifeline systems that generally transport sewage, water, oil, and natural gas. The relative displacement between the soil and the pipeline make the seismic behavior of buried pipelines distinct from most above-ground structures. A buried pipeline can extend for a long distance and pass through different types of soil having different properties; thus, during an earthquake, one pipe can experience different types of ground motion along its length. Major seismic hazards which can significantly affect a pipeline system include ground failure (permanent ground deformation) and ground motion (transient ground deformation). Seismic wave excitation of the ground can cause buried pipelines to experience additional stress.

Site effects can strongly affect the seismic response of a structure. Topographic irregularities are a type of site effect that can significantly affect the seismic site response and the performance of pipelines. The effect of topography on seismic excitation can result in damage to structures built on slopes and cause avalanches

(Athanasopoulos et al. 1999; Hancox et al., 2003; Khazai and Sitar 2003; Sepúlveda et al., 2005a, Sepúlveda et al., 2005b) and landslides (Nakileza and Nedala 2020). In the recent past, numerous seismic motion records and observed earthquake damage have pointed towards topographic amplification as an important factor affecting damage to structures (Davis and West 1973; Griffiths and Bollinger 1979; Pedersen et al. 1994; Hartzell et al. 1994; Spudich et al. 1996; Chavez-Garcia et al. 1996; Le-Brun et al. 1999; Caserta et al. 2000; Graizer 2009; Massa et al., 2010; Marzorati et al. 2011; Buech et al. 2010; Meslem et al. 2012; Assimari and Jeong, 2013; Hailemi-kael et al. 2016; Khan et al. 2020). Additionally, a number of numerical and theoretical studies have investigated this phenomenon (Boore et al. 1981; Paolucci 2002; Nguyen and Gatmiri 2007; Graizer 2009; Lovati et al. 2011).

A review of observation records and experimental studies and their comparison with theoretical and numerical results can be found in Geli et al. (1988) and Massa et al. (2014). These studies suggest that the amplification observed to be caused by the topographic effect reached a value of 10 and that analytical solutions and numerical methods available for site-specific problems significantly under-predicted the observed

* Correspondence: m.bastami@iiees.ac.ir
[2]International Institute of Earthquake Engineering and Seismology, Tehran, Iran
Full list of author information is available at the end of the article

amplifications. The results of some recent numerical studies have estimated even higher values for amplification due to the topographic effect (Mitani et al. 2012). In other cases, the results of numerical research have been consistent with the observed results (Mayoral et al. 2019).

Although a number of studies have been carried out to model and predict the effect of topography on seismic amplification, it is still not entirely understood (Rizzitano et al. 2014; Shabani and Ghanbar, 2020). A few international seismic building codes have addressed the subject of topographic amplification; however, this phenomenon has not been considered in design guidelines, attenuation relations, or hazard maps of pipelines.

After the Northridge earthquake in 1994, O'Rourke and Toprak (1997) investigated the influence of site effects on buried water pipelines. They analyzed the amount of pipeline restoration using GIS maps and concluded that the most severe damage to pipelines occurred on hills. Isoyama et al. (2000) studied water pipeline systems after the Kobe earthquake and offered an amplification factor to accommodate the topographic effect. Kimiyasu and Tatsuo (2004) evaluated damage to water pipelines after the Kobe earthquake and concluded that slopes and pipeline branching had the great effects on the damage potential to pipelines. Prodromos (2012) and Tromans (2004) emphasized the importance of the topographic amplification effect on the behavior of pipelines in seismic events. The current research was undertaken to study pipeline behavior under seismic excitation when considering the effect of topography.

Methods
Models used
The model geometry used included double-faced slopes with pipelines. The surrounding soil medium was developed using the general-purpose finite element (FE) code program in ABAQUS (2012). The operation of the pipelines subjected to topographic effects were investigated by placement of a pipeline at the crest or toe of a slope or by running the pipeline along a hillside and crest as a function of topography.

For a pipeline at the crest or toe of a slope, the interaction between the soil and the pipeline is an important factor for which two-dimensional (2D) analysis is suitable. When running the pipeline up a hillside or over crest, in addition to the interaction, the curvature of the pipeline at the bottom and top of the slope makes determination of the bending of the pipe an additional factor for consideration. For this condition, the model should be three-dimensional (3D).

Because it is difficult for a beam model to analyze large deformation in pipe cross-sections as well as the interaction with the surrounding soil, a shell element was used to model the pipeline system in both the 2D and 3D models. The FE shell model has been previously proposed for this purpose (Behnamfar et al. 2013; Datta, 1999; Duhee et al. 2020; Kouretzis et al. 2006; Saberi et al. 2011, 2015; Takada and Higashi 1992; Oskouei and Ghaznavi, 2017; Rahimi et al. 2019).

Mitani et al. (2012) emphasized the ability of ABAQUS to investigate topographic effects on the amplification of seismic motion. Some building codes (BS EN 2004; The Iranian Code of Practice for Seismic Resistant Design of Building 2015) indicate that topographic effects are important for hills having an elevation of over 30 m. Accordingly, the height of the slopes was selected to be 50 m.

Material characteristics
In this research, the effect on pipelines of slope instability which leads to permanent ground deformation was not investigated. Therefore, a soil profile was selected that avoided instability and slippage. The specifications were based on experiments carried out on tuff and shale rock in the cities of Sanandaj and Saqqez in Iran. The main line for Iranian gas transport to Turkey passes through the Sanandaj-Saqqez axis. The aim of using different specifications was to investigate the effect of changes in the shear wave velocity on the slope and pipeline performance.

The soil medium included four types of homogenous tuff and shale material: R1, R2, R3, and R4. Table 1 presents the specifications of the soil types. Materials R1 to R3 were used only for analysis of the effect of the soil on the amplification of axial strain in the pipe. Mohr–Coulomb models were used for the seismic effects common to the region and elastic models were used for the infinite boundary elements. The ability of Mohr–Coulomb models to estimate topographic effects has been confirmed by Mitani et al. (2012). To ignore the effect of impedance on the results, the stiffness of the infinite parts was set to be the same as for the finite parts.

The pipe was composed of steel and exhibited inelastic behavior. The yielding condition followed the von Mises yield criterion for isotropic/kinematic hardening. The pipe specifications were extracted from American Petroleum Institute Specification for pipeline (2000) and are summarized in Table 2. When investigating the effect of pipe stiffness on its seismic performance, diameter-to-thickness (D/t) values of 40, 50, 99 and 129 were evaluated.

Material damping was of the Rayleigh type and used coefficients α and β for mass and stiffness-proportional damping, respectively. These coefficients were computed from the results of modal analysis to identify the modes making major contributions. A damping ratio of 3%, formerly adopted by Qi (2011), was employed to carrying out the slope simulation.

Table 1 Characteristics of soil medium

Rock type	R1	R2	R3	R4
Description	shale	shale	tuff	tuff
Cohesion C (kPa)	30	36	31	32
Internal friction angle φ (deg.)	27	30	30	32
Modulus of elasticity E (Pa)	1.00E+ 9	2.02E+ 9	3.15E+ 9	4.27E+ 9
Mass density (kg/m³)	2200	2250	2320	2350
Poisson ratio υ	0.28	0.28	0.27	0.26
Dilatant angle φ (deg.)	2	3	4	4
Shear wave velocity (m/s)	421	592	731	849

Dynamic loading

The main characteristics of the strong motions selected were earthquake magnitude, shear wave velocity of the soil on which the motion was recorded, and frequency content. This study determined the time history response of the pipes under the effect of topography due to seismic loading, which required the selection and application of suitable ground motions for the model.

For selection of ground motion, the Pacific Earthquake Engineering Research Center (n.d) strong motion database was consulted. Modal analysis had previously been conducted for each soil category and the range of frequencies having large mass participation factors was calculated using linear perturbation analysis. This was compared to the strong frequency band of the Fourier amplitude spectrum of each record examined. Table 3 shows the motions chosen for similar soil types having frequency bands that were sufficiently strong (magnitude > 6).

Records from the Northridge (1994) and Chi-Chi (1999) earthquakes were examined for this purpose. The characteristics of the selected records are summarized in Table 3. The spectra of ground motion are shown in Fig. 1. In order to investigate the dependence of the pipeline and the slope response on the incoming wave frequency, a harmonic wave with a duration of 10 s and amplitude of 0.8 g was applied at frequencies of 1, 3, 5, 7 and 9 Hz as input waves.

Mesh size

To avoid the filtering out of the high-frequency components of the seismic input motion during propagation and ensure the accuracy of the numerical solution, the length of the elements of the mesh was selected as:

$$1 \le \left(\frac{1}{8} \text{ to } \frac{1}{5}\right) \frac{V_s}{f_{max}} w \le 5l \tag{1}$$

where w and l are the width and length of the elements, respectively, in the direction of wave propagation and f_{max} is the maximum frequency of the input motion (Rizzitano et al. 2014). The explicit solution is stable if the maximal time step size Δt is smaller than the critical time step size Δt^{cr}, for which the criterion is:

$$\Delta t^{cr} = \frac{l}{V_s} \tag{2}$$

Where V_s is the wave propagation velocity (Li et al., 2019: Courant et al. 1928: Kuchleme and Lysmer 1973).

The lengths of most elements used in analysis was 0.85 m; however, to study the sensitivity of pipe strain versus increment time of input motion, harmonic motion with an amplitude of 0.8 g and frequency of 3 Hz was applied with a shape factor of 0.7 and diameter-to-thickness (D/t) ratio of 99. The time increment was set at 0.2, 1 and 5 times 0.001 (i.e. 0.0002, 0.001 and 0.005 s). The results of analysis of the three models are presented in Fig. 2 and show that the difference in pipe strain is about 2%; thus, the time step was selected to be 0.001 s.

Soil-pipeline interaction

A contact surface algorithm was employed to model the soil-pipeline interface in which sliding and soil-pipe separation were made possible using the contact function. This contact capability allows finite sliding and separation between two surfaces based on the Coulomb friction criterion. The reduced interface

Table 2 Pipe characteristics

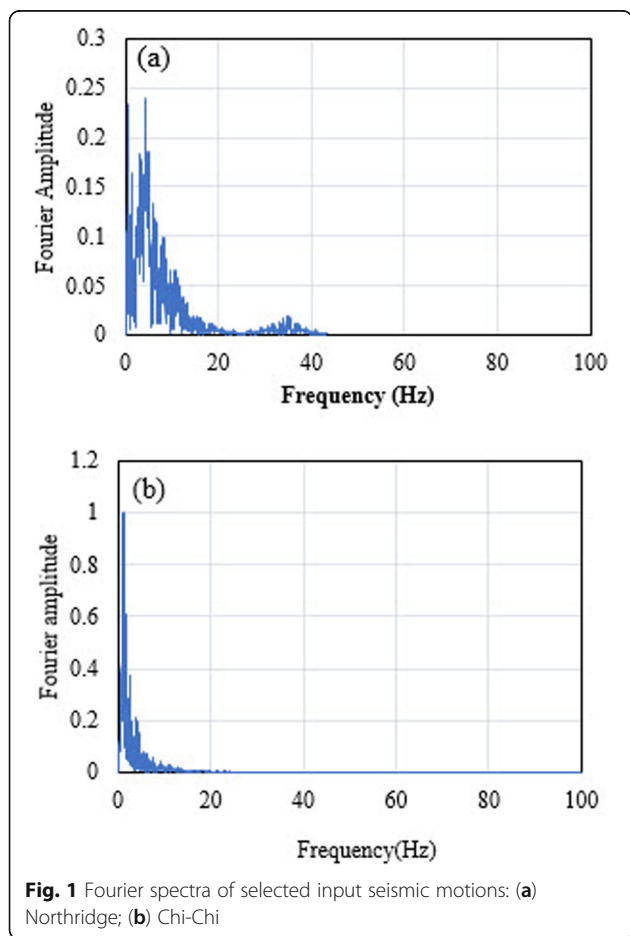| Pipe type	Diameter D (cm)	Thickness (cm)	Burial depth (m)	Mass density (kg/m³)
Steel APIX65	101.6 (40 in)	1.03 (0.406 in)	1.5	7850
Modulus of elasticity E (Pa)	Poisson ratio (υ)	Yield stress σ_y (Pa)	Ultimate stress σ_u (Pa)	
210E+ 9	0.30	465.4E + 6	517.7E + 6	

Table 3 Characteristics of ground motions used

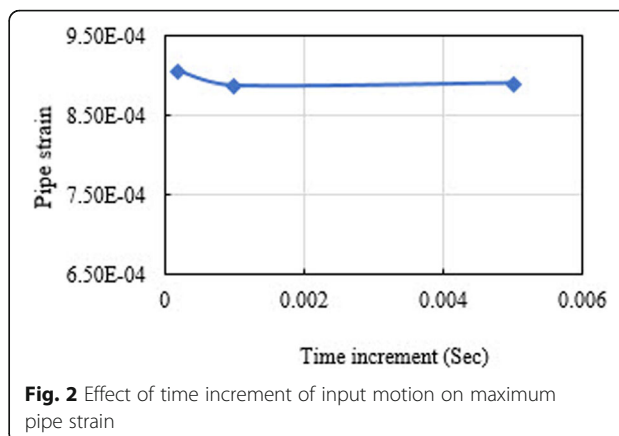| Earthquake	Station	V_s	PGA
Chi-Chi	CHY080	469	**0.902**
Northridge	Santa-Monica	609	**0.883**

friction angle between the soil and pipe was set at 0.75 of the internal friction angle of the soil (φ), as suggested by Yimsiri (2004).

Modeling of far-field soil medium

In order to simulate the far-field effect, infinite elements were employed instead of the use of absorbing boundary conditions such as springs and dampers. This approach overcomes difficulties with the absorbing boundary conditions and requires less memory and computation time. The nodal points in each infinite element are located on the interface with the FE region. The nodes pointing toward the infinite direction are positioned far enough away to enhance the performance of the infinite elements.

Fig. 2 Effect of time increment of input motion on maximum pipe strain

2D model

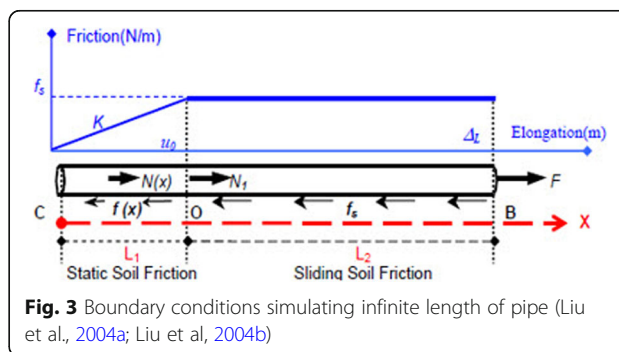The bottom and sides of the model were set as infinite elements to increase the functionality of the model slope.

3D model

All sides of the model were set as infinite 3D elements. The bottom of the model continued up to a depth of 40 m and the base was set as seismic bedrock.

3D modeling of far-field pipeline

To produce a realistic estimation of the dynamic response, it was necessary to model the infinite length of the pipe away from the toe of the slope. This was possible by extending a limited length of pipe from the toe to a suitable boundary condition. In this research, the boundary condition proposed by Takada et al., 2001 was adopted. They assumed that lateral deformation of distant portions of the pipeline will not affect the response of the portion under study, but that longitudinal friction is important.

Fig. 3 shows the friction force along part *OB* of the pipe due to axial force *F* consisting of static friction *OC* and slip friction *CB*. The relation of *F* to extension ΔL is used to introduce a nonlinear spring at the pipe boundary as:
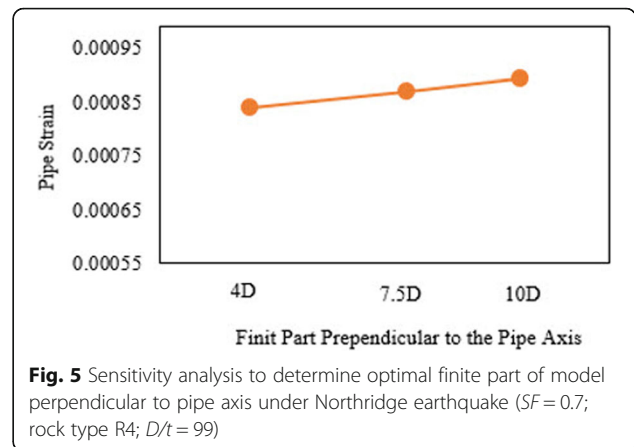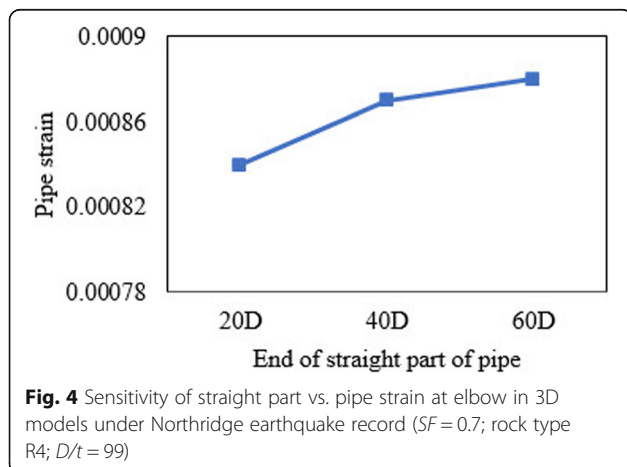

Fig. 1 Fourier spectra of selected input seismic motions: (**a**) Northridge; (**b**) Chi-Chi

Fig. 3 Boundary conditions simulating infinite length of pipe (Liu et al., 2004a; Liu et al, 2004b)

Elyasi *et al. Geoenvironmental Disasters*   (2021) 8:22

Page 5 of 14

$$F(\Delta L) = \begin{cases} \sqrt{\dfrac{3EAf_s}{2}U_0\Delta L^{\frac{2}{3}}} \;\; 0 \le \Delta L \le U_0 \\ \sqrt{2EAf_S\left(\Delta L - \dfrac{1}{4}U_0\right)} \; U_0 \le \Delta L \le \dfrac{\sigma_y^2}{2Ef_s} + \dfrac{U_0}{4} \end{cases} \quad (3)$$

where E is the elastic modulus, A is the pipe cross-section, f_s is the slip friction force on the unit length of the pipe, U_0 is the yield displacement, and σ_y is the yield stress on the pipe material.

A number of sensitivity analyses were employed to determine the sufficient and optimized length of the pipe legs when modeling slopes for $SF = 0.7$ and rock type R4. In this context, straight lengths 20D, 40D and 60D were selected to simulate the shell parts in the elbow branches. The effect of the shell length on the maximum axial strain on the pipeline elbows is shown in Fig. 4. It can be seen that the difference between the axial strains for the three shell lengths was less than 4%. As a result, length 40D was considered to optimize the computational time and provide satisfactory accuracy.

Sensitivity analysis was employed to determine the optimal finite part of the model perpendicular to the pipe axis. According to Wolf (1985), modeling of a soil medium up to a distance from the center of a pipe that is equal to four times the diameter will produce an accurate response for pipe-soil system analysis. In the current study, models with distances of 4, 7.5 and 12 times the diameter from the center of the pipe were compared and the results are presented in Fig. 5. As seen, the difference between the strains in the models was about 5%; thus, the model was extended by FE up to 7.5 times the diameter of the pipe. Examples of the 2D and 3D models used in the analyses are presented in Figs. 6 and 7.
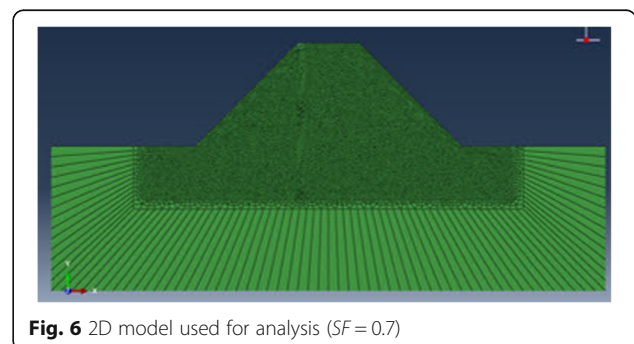

Fig. 5 Sensitivity analysis to determine optimal finite part of model perpendicular to pipe axis under Northridge earthquake ($SF = 0.7$; rock type R4; $D/t = 99$)
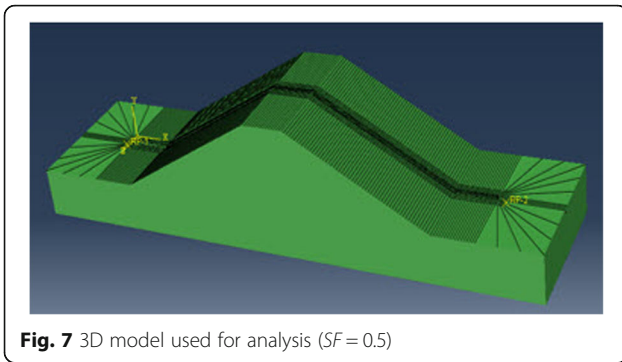
Results

Amplification of input motion and crest/ toe strain ratio of pipeline due to topography

In this research, topographic amplification is defined as the peak ground acceleration (PGA) for the crest to toe of the slope. To investigate the topographic effects on the amplification of a seismic wave, the hills were modeled in 2D at height-to-half-width for SF values of 0.3, 0.5, 0.7, 0.9 and 1.7 (equivalent to a 60° slope). The rock type was R4. The results are shown in Figs. 8 and 9 for a harmonic wave with 0.8 g of amplitude and the Chi-Chi and Northridge records, respectively.

As seen, as SF increased, the amplification of the seismic wave increased. Maximum amplification occurred when the frequency of the input motion was 3 to 5 Hz, which is in good agreement with the natural frequency of the slopes. In this study, the strain ratio denotes the strain on a pipeline located at the crest of the topography to the strain at the toe. To analyze the effect of slope on pipeline performance, the results of models in which the pipeline is located at the crest were compared with those in which the pipeline was located at the toe. The crest-to-toe ratio of the strain is presented in Fig. 10 for the Chi-Chi and Northridge earthquakes.

As seen, the maximum amplification of seismic acceleration was 6.2. When the maximum radial strain ratio in models for which the pipeline was located at the top


Fig. 4 Sensitivity of straight part vs. pipe strain at elbow in 3D models under Northridge earthquake record ($SF = 0.7$; rock type R4; $D/t = 99$)

Fig. 6 2D model used for analysis ($SF = 0.7$)

Fig. 7 3D model used for analysis (*SF* = 0.5)

Fig. 9 Effect of *SF* on amplification of seismic input motion (Chi-Chi and Northridge)

of the slope was compared with the strain of the pipeline located at the bottom of the slope, the value was 113 for the Chi-Chi earthquake at D/t = 129. It should be noted that the D/t of the pipeline, which is directly related to the stiffness of the pipe section, has an important effect on the strain ratio of the pipe. By increasing the D/t from 40 to 129, the maximum strain ratio changed from 63 to 113 at SF = 1.7. Another important factor relating to the strain ratio is the SF of the slope. At SF = 0.3, the strain ratio for models having a pipeline near the top of the slope was compared with those having pipelines near the bottom of the slope. This value was about 7; however, as the SF increased, the strain ratio increased.

Effect of soil characteristics (shear wave velocity) on seismic response of pipelines at crest
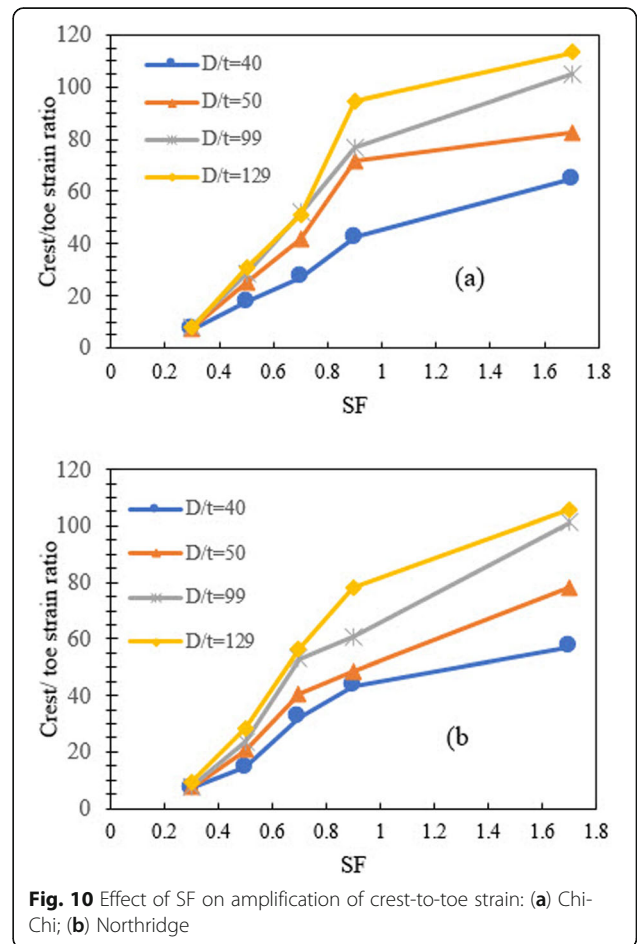
The evaluation criterion from American lifelines alliance (ALA) (2001) was used to evaluate the performance of the pipelines against wave propagation.
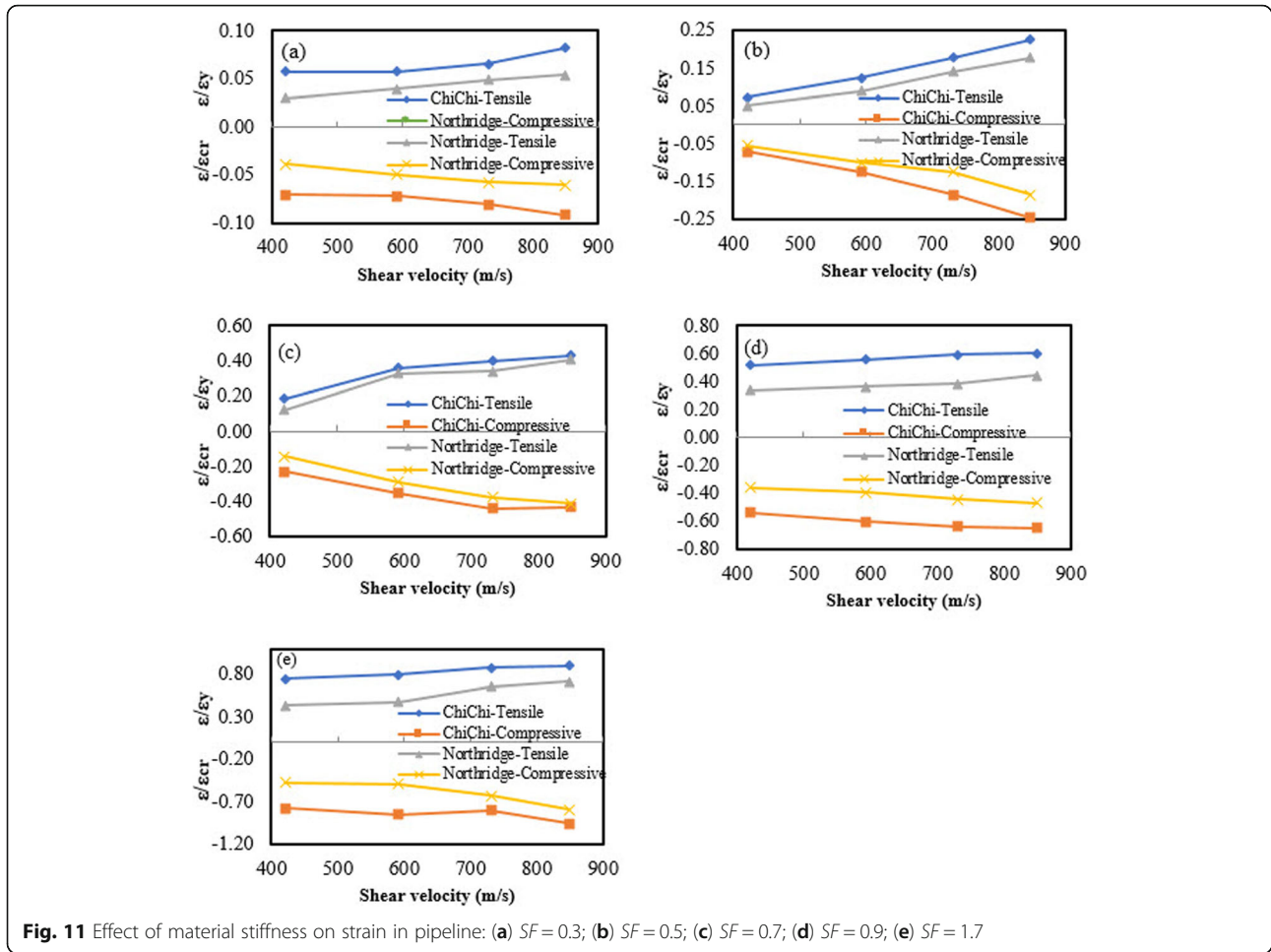
ALA suggests a critical strain limit of 0.5% in tension and uses the formula shown in Eq. (4) for compression. In this research, however, the strain was normalized to the critical and yield strains (ε_{cr} and ε_y) for compressive and
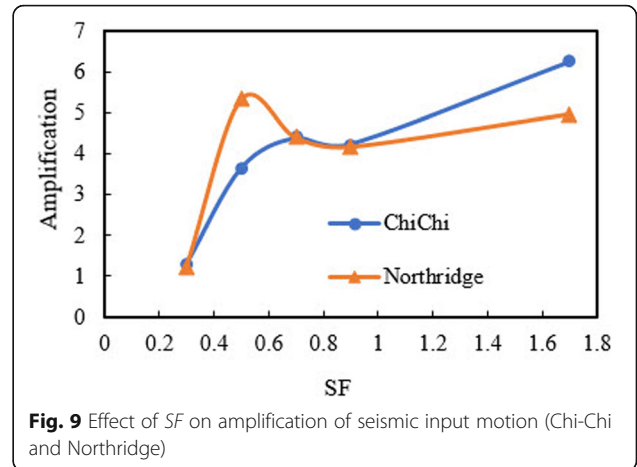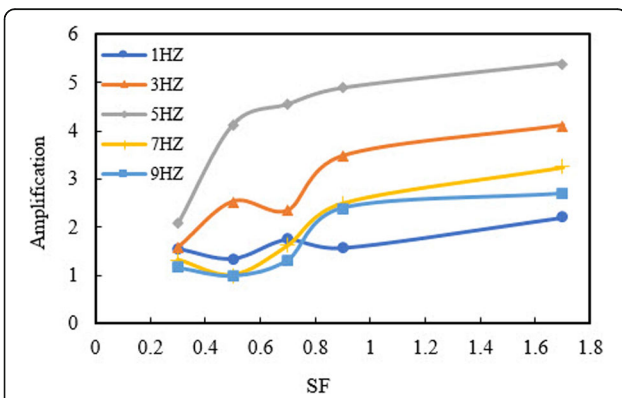
tensile strain, respectively. The yield strain was evaluated using Hook's law and was calculated to be about 0.002.

$$\varepsilon_{\text{Critical}}^{\text{WavePropagation}} = 0.75\left[0.5\left(\frac{t}{D'}\right) - 0.0025 + 3000\left(\frac{pD}{2Et}\right)^2\right]$$

(4)

Fig. 10 Effect of SF on amplification of crest-to-toe strain: (**a**) Chi-Chi; (**b**) Northridge

Fig. 8 Effect of *SF* on amplification of seismic input motion (harmonic motion amplitude = 0.8 g) at various frequencies

Fig. 11 Effect of material stiffness on strain in pipeline: (**a**) *SF* = 0.3; (**b**) *SF* = 0.5; (**c**) *SF* = 0.7; (**d**) *SF* = 0.9; (**e**) *SF* = 1.7

$$D' = \frac{D}{1 - \dfrac{3}{D}(D - D_{min})}$$

The results for the Chi-Chi and Northridge earthquakes at $D/t = 99$ for different values of SF is presented in Fig. 11. The most important seismic parameter, shear wave velocity, was used to define the stiffness of the material. It can be seen that, as the stiffness of the soil medium increased, the normalized strain increased. This could be the result of reduced slippage between the surrounding soil and the pipeline. An increase in the stiffness of the soil medium increased the rate of increase in the strain. To evaluate the response of pipelines to variations in the stiffness of the soil medium due to harmonic wave motion, a harmonic motion of 0.8 g and period of 0.333 s (3 Hz) was considered. The results are presented in Fig. 12 and indicate that the rate of increase of the strain increased as the stiffness of the soil medium increased.

Effect of shape factor *SF*

Models of rock type R4 at $D/t = 99$ with different SF values and seismic motions were analyzed to determine the effect of the SF of the topography on pipeline strain. The results are presented in Fig. 13 and indicate that an increase in SF increased the normalized strain on the

Fig. 12 Maximum strain of pipelines vs. shear wave velocity of soil medium by *SF* value
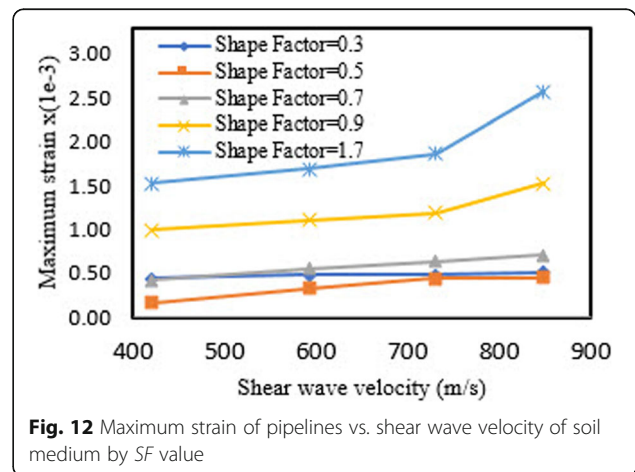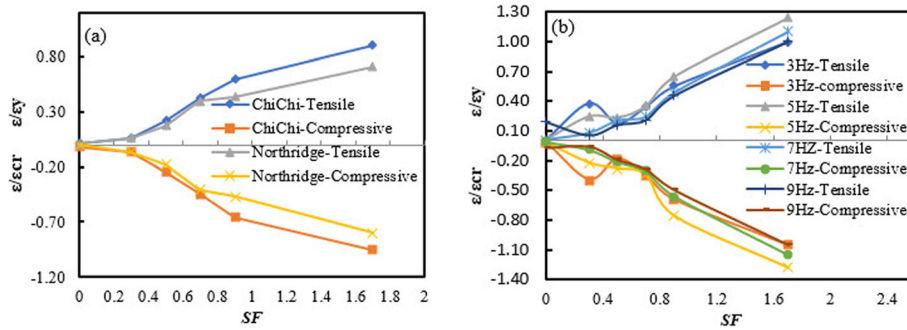
Fig. 13 Effect of *SF* on pipeline strains: (**a**) Chi-Chi and Northridge input motion; (**b**) harmonic input motion at PGA = 0.8 g
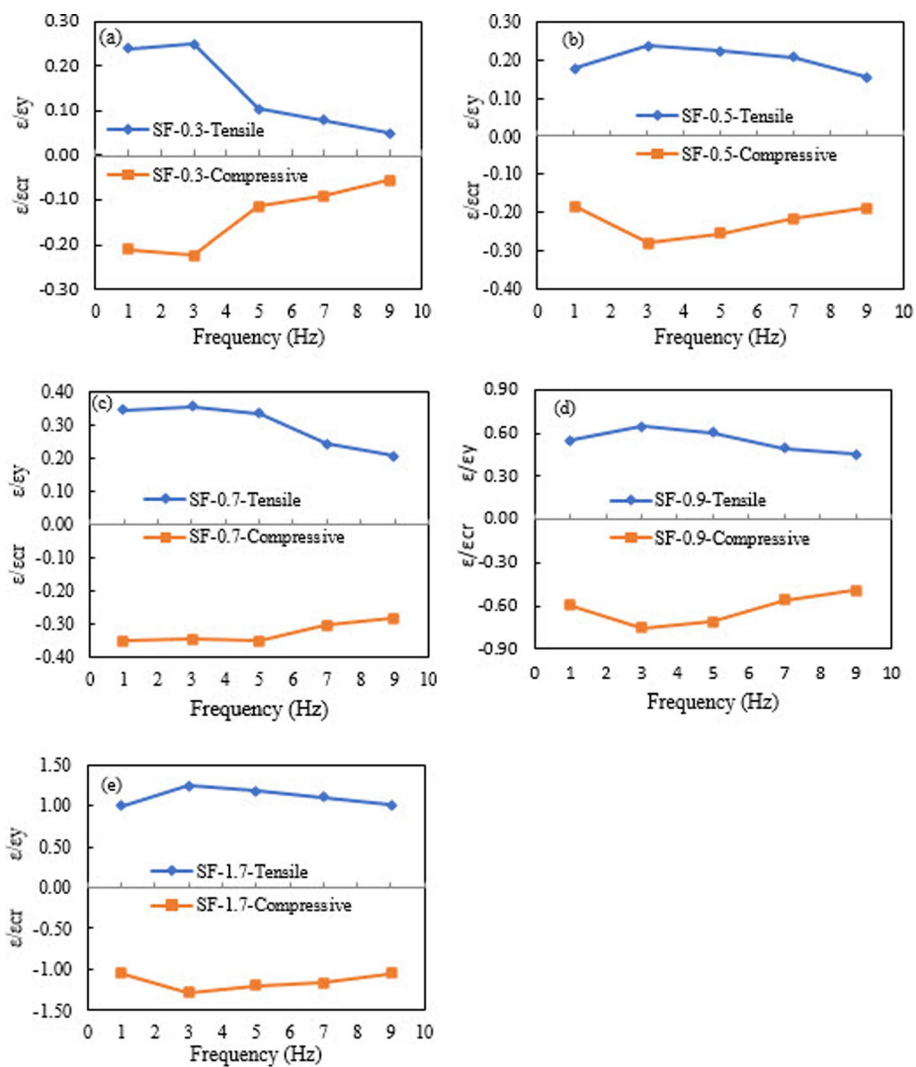
Fig. 14 Effect of frequency of input motion on pipeline strain for rock type R4: (**a**) *SR* = 0.3; (**b**) *SR* = 0.5; (**c**) *SR* = 0.7; (d) *SR* = 0.9; (**e**) *SR* = 1.7

pipelines. At *SF* = 1.7, the tensile and compressive strains of the pipeline exceeded the yield and critical strains for harmonic motion.

Effect of frequency content of input motion

To investigate the effect of the frequency content of the input motion on the response of pipelines, harmonic motion with an amplitude of 0.8 g and duration of 10 s was applied at different frequencies. The rock type was R4 and *D/t* = 99. The results presented in Fig. 14 indicate that, in all models, the maximum normalized strain for harmonic motion occurred at a frequency of about 3 Hz. This is in good agreement with the natural frequency of the topography, which was about 3 Hz at *SF* = 0.3, the natural frequency of the model.

Results of 3D models

The performance of longitudinal pipelines running through topography was studied to evaluate the effect of *SF* and the shear wave velocity of the environment. Because the pipeline passes through different topographical features, the need for periodic visits, repairs and inspections prevented the operating slope from exceeding a specific level. Therefore, the maximum ratio of the shape studied in the 3D models was set at 0.7 (35° slope).

Effect of *SF* on seismic response of pipelines

Figure 15 shows the maximum axial strain ratio versus *D/t* at *SF* values of 0.3, 0.5 and 0.7 at the elbows located at the crest and toe of the slope for the Chi-Chi and Northridge input motions. As seen, the rate of change of the strain ratio at *SF* = 0.7 was much higher than for the 0.5 and 0.3 ratios, (rock type R4). Figure 16 shows that, for the R1 material at *D/t* = 99, the amount of strain at the elbow at the crest of the slope was much higher than at the toe.

Effect of shear wave velocity (stiffness) on the seismic response of pipelines

The maximum radial strain of the pipeline was investigated at the toe and crest of the model at *SF* values of 0.3, 0.5 and 0.7. Figure 17 shows that, as the shear wave velocity of the environment increased, the axial strain ratio increased to maximum critical strain. However, following the increase in material hardness, this ratio decreased gradually. This could be the result of a decrease in displacement between the pipeline and the surrounding medium and the proximity of the natural frequency of the structure to the frequency of the input motion. It should be noted that most strain due to the topographic effects occurs at the pipe elbows.
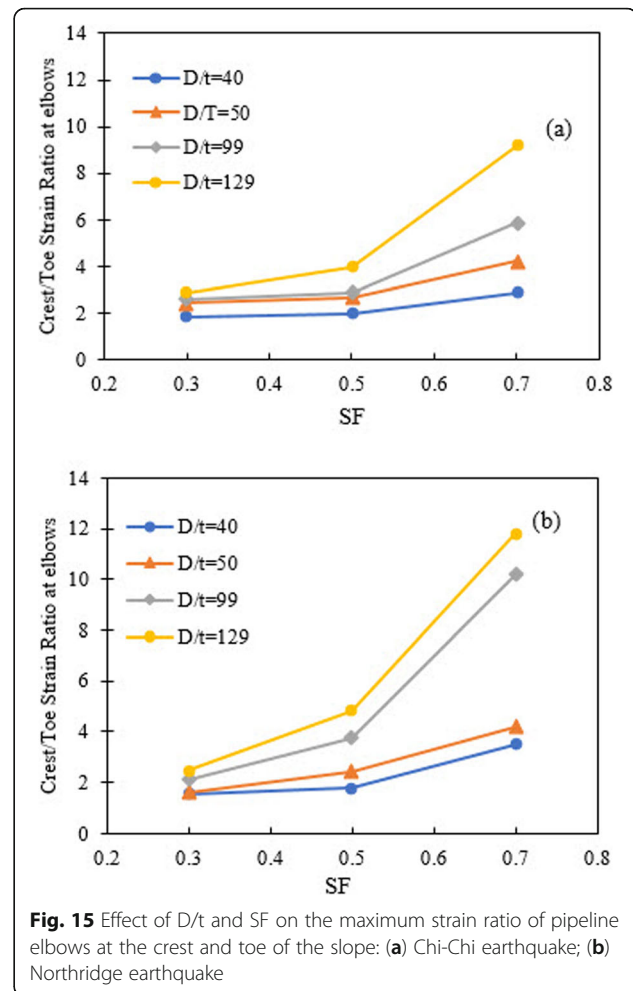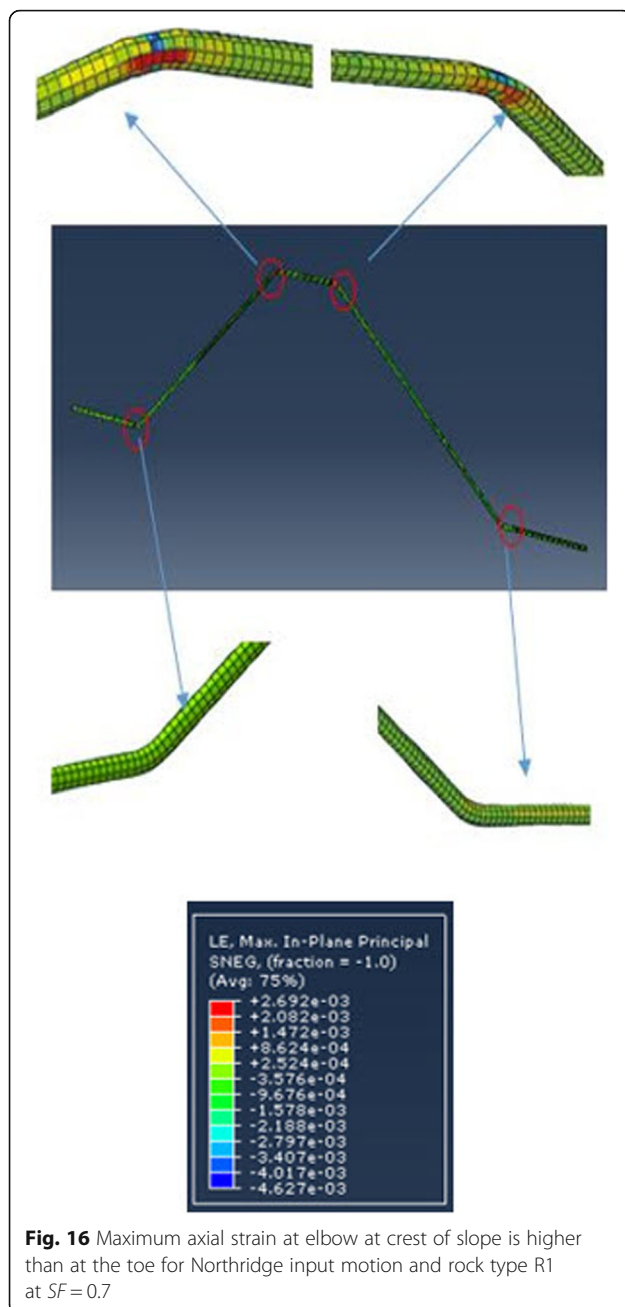

Fig. 15 Effect of D/t and SF on the maximum strain ratio of pipeline elbows at the crest and toe of the slope: (**a**) Chi-Chi earthquake; (**b**) Northridge earthquake

Discussion

Observation and field studies have revealed that the magnification of a seismic wave caused by the effect of topography can, in some cases, reach a value of 10 (Massa et al. 2014). The results obtained in the present study produced a maximum amplification of about 6.2. The magnification rate is a function of the dominant frequency of the input wave and its degree of adaptation to the natural frequency of the topographic impediment. In such a case, harmonic input waves with frequencies of 3 to 5 Hz obtained the highest magnification and this frequency limit corresponded to the natural vibrational frequency of the slope.

Another important factor affecting the magnification rate was the shape factor of the impediment. An increase in SF was found to increase the amplification ratio. The results of most numerical research have shown that the maximum amplification ratio in numerical investigations was 250% (Massa et al. 2014; Lovati et al., 2011); however, the results of the present study revealed much greater values that were consistent with the results reported by Mitani et al. (2012).

Fig. 16 Maximum axial strain at elbow at crest of slope is higher than at the toe for Northridge input motion and rock type R1 at $SF = 0.7$

The performance of pipelines subjected to topographic effects were investigated by placement of the pipeline at the crest or toe of a slope or by running the pipeline along a hillside or crest as a function of the shape of the topography. In the former condition, 2D models were used. In the latter condition, determination of the strain of the pipeline at the bottom and top of the slope became an important consideration; thus, the 3D modeling was used.

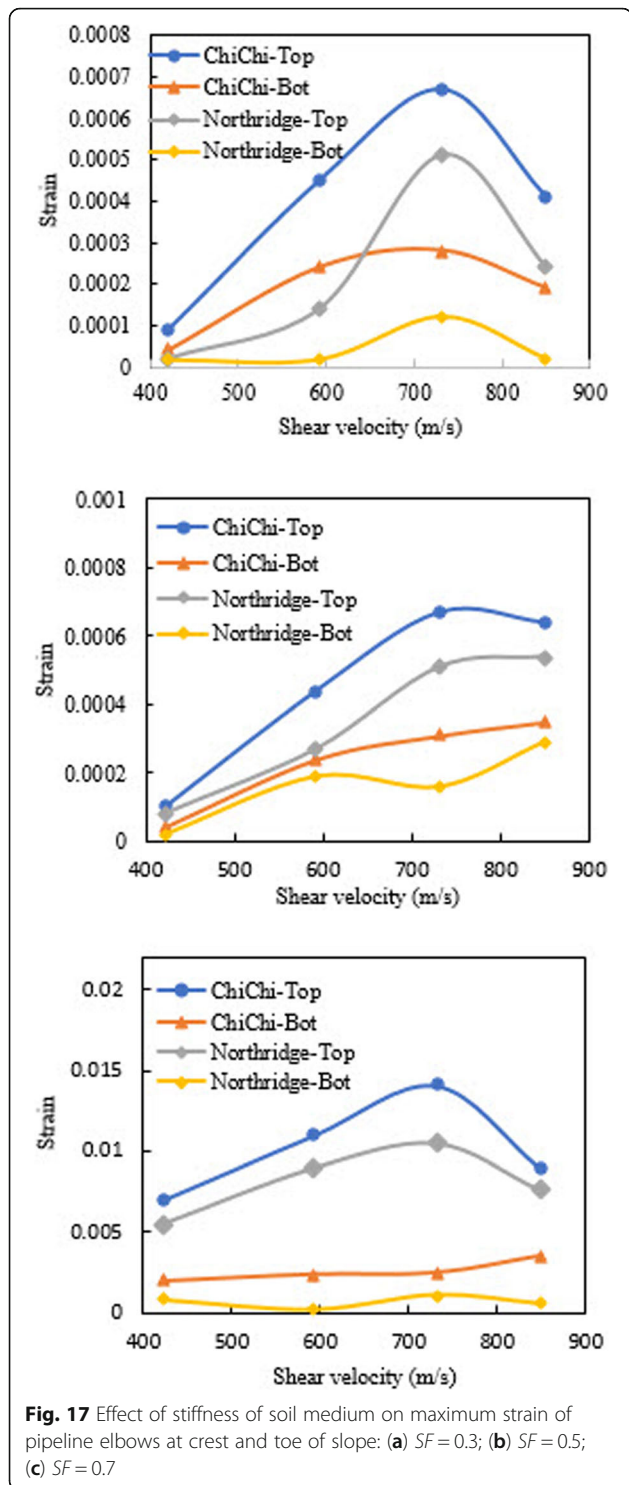Because the goal was to study the topographic effect on pipelines, the properties of the materials selected were those that did not cause general instability on the slope. Under such conditions, displacement of the slope itself would be much greater than displacement at the toe of the slope. In 2D models, however, the maximum strain on the pipeline at the crest of the topography was affected simultaneously by the maximum displacement at the edge of the slope and acceleration magnification. The vibration and displacement were in the direction of the cross-section of the pipeline and the strain on this section primarily coincided with displacement of a slope exhibiting less stiffness compared to the longitudinal direction. Thus, the crest-to-toe strain ratio varied from 7 to 113 at SF values of 0.3 to 1.7.

In 3D models (Fig. 15), the maximum strain ratio of the pipe bend at top of the slope compared to that at the bottom of the slope was about 10 for Chi-Chi and 12 for Northridge. This corresponds to the maximum values in the 2D models of 51 and 56, respectively. Because the pipeline passes through different topographical features, the need for periodic visits, repairs and inspections prevented the operating slope from exceeding a specific level. Therefore, the maximum ratio of the shape studied in the 3D models was set at 0.7. In fact, under these conditions, the directions of vibration and displacement ran parallel to the longitudinal axis of the pipeline and the much greater stiffness in this direction caused the strain of the pipe to be more in line with acceleration. Therefore, the results were synchronized with the maximum acceleration amplification.
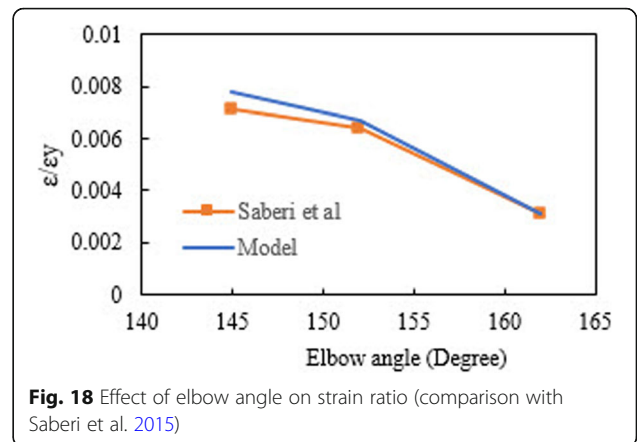
The elbows are the most critical parts of pipelines under seismic wave propagation loading. The results of studies such as those by Saberi et al. (2015) have shown that strain in pipelines at the bends, regardless of the topographic effect, can exceed critical values, depending on the angle of the bend and the type of input wave.

In the present study, limit values selected were based on American lifelines alliance (ALA) (2001). In the 3D models, the greatest axial strain occurred at the bends of the pipes. In fact, the simultaneous effect of horizontal displacement at the slope crest and magnification of the maximum acceleration at the pipe bend, which is actually the most vulnerable part, was the cause of this. Although successive changes in compressive and tensile axial strain occurred on the slope of the relief, the magnitude compared to strain at the elbows was negligible. Observation of the topographic effects of past earthquakes has revealed that the amplification effects were negligible along the slope of the relief (Massa et al. 2014).
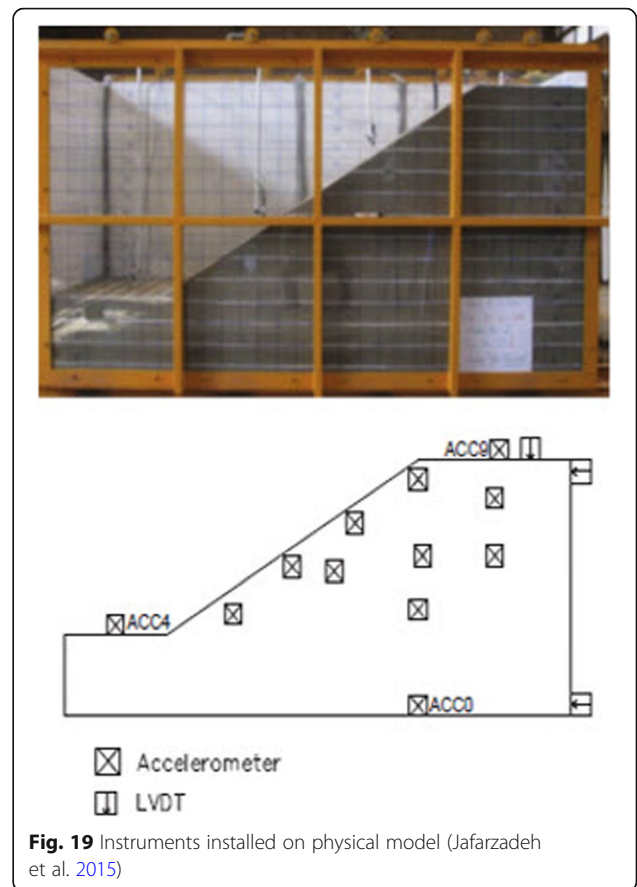
The performance of a pipeline at a bend depended on a range of parameters, including the diameter-to-thickness ratio, the characteristics of the frequency content of the input motion, and the angle of the pipe bend. In this study, the strain values at the elbows changed with changes in the type of soil, rock environment, input motion, SF, and D/t in the 3D models.

Fig. 17 Effect of stiffness of soil medium on maximum strain of pipeline elbows at crest and toe of slope: (**a**) SF = 0.3; (**b**) SF = 0.5; (**c**) SF = 0.7

Fig. 18 Effect of elbow angle on strain ratio (comparison with Saberi et al. 2015)

The Iranian Code of Practice for Seismic Resistant Design of Building, suggests 1.1–1.4 for the lower bound of the topographic effect as a potential geotechnical hazard. Modern seismic design codes for lifelines, however, have failed to consider topographic effects as a potential geotechnical hazard, although they can pass through a wide range of geotechnical conditions, especially topographies. For example, the latest version of the loading and seismic analysis guidelines for Iranian lifelines Code 600 (2012) considers only liquefaction, ground sliding due to

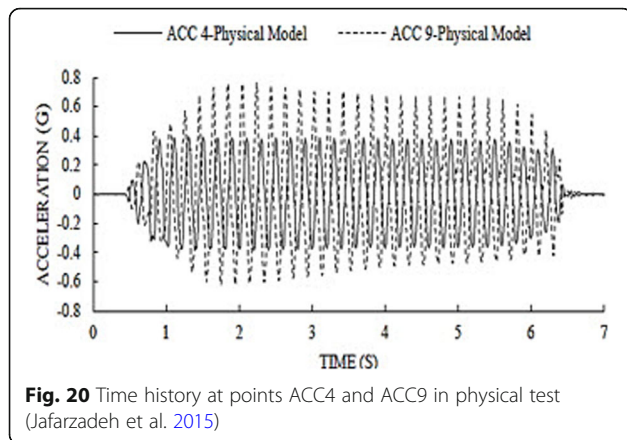**Fig. 19** Instruments installed on physical model (Jafarzadeh et al. 2015)

Topographic effects have been incorporated into some modern building codes. For example, horizontal amplification factors of 1.1–1.6 for convex topography have been suggested in the Seismic Code of China GB50011 (2010) and 1.2–1.4 has been suggested in BS EN (2004).

Fig. 20 Time history at points ACC4 and ACC9 in physical test (Jafarzadeh et al. 2015)

permanent ground displacement, and fault rupture as geotechnical threats.

The results of the 2D and 3D models in the present study indicate that the topographic effect must be incorporated into seismic design codes for buried pipelines. The failure to take topography-related amplification into account for the seismic design of pipelines could result in severe damage to pipelines during earthquakes. The topographic amplification factors presented in building codes are generally lower than the results of the present study and experimental observation from past earthquakes.
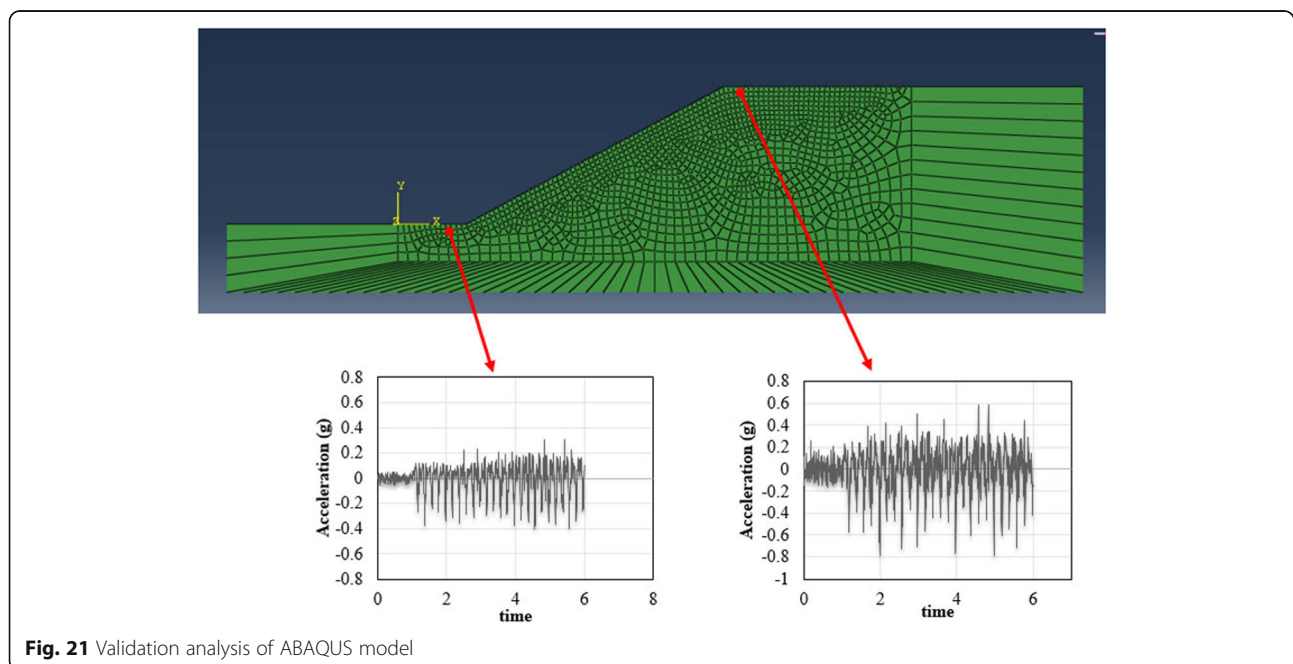
Verification

To evaluate the reliability of the model when modeling the performance of a pipeline, the axial strain-to-yield strain ratios at the elbow of a pipeline located at the bottom of a hill for *SF* values of 0.3, 0.5 and 0.7 were compared with the results obtained by Saberi et al. (2015) at the same *D/t* ratio and a shear wave velocity similar to that of the Chi-Chi earthquake. The topographic effect at the elbow located at the base of the hill was negligible. The results are presented in Fig. 18.

To validate the reliability of the models used for the topographic effect, shaking table test results for a physical slope model on a small scale of 1 g were obtained (Jafarzadeh et al. 2015). The amplification of seismic acceleration at the slopes was used as the reference criterion (Figs. 19 and 20). A corresponding ABAQUS slope model was built using the same geotechnical parameters under infinite element boundary conditions (Fig. 21). A harmonic 6-s motion with an amplitude of 0.3 g was used as the input motion to insure a similar PGA. The results indicated that, at the bottom of the slope, the peak value of acceleration was about 1.3 times higher than that of the input wave. At the top of the slope at the crest, the peak value was about 2.6 times higher than that of the input wave and the waveform was almost the same as that at the toe. All the results show that this method is practically acceptable.

Conclusion

Researchers have studied topographic effects in recent decades as part of site-effect investigations. In the current study, double-faced slopes were modeled and the topographic effects were compared with the results of numerical and field research. Next, the performance of pipelines running near the crest of a slope and the effect of topography were investigated using 2D models.

Fig. 21 Validation analysis of ABAQUS model

The strain ratio of a pipeline running near the crest was compared with that of one running near the toe and with the amplification factor. Pipelines crossing the slope were modeled in 3D and their behavior was evaluated. Specifically, bends in the pipes, as the most critical zones at the top and bottom of a slope, were compared and the following results were obtained:

1. The amplification ratio at the crest of a slope was greater than at the bottom of the slope. This amplification ratio is a function of the dominant frequency of the input wave and its degree of adaptation to the natural frequency of the topographic impediment, the shape factor (SF), and the material properties.
2. The maximum amplification of motion was about 6. The crest-to-toe strain ratio, which is the radial strain of the pipeline at the crest of the slope to that at the toe, for 2D models varied from 7 to 113. This varied according to the SF and the D/t of the pipeline as well as other factors and indicates the importance of the topographic effect on pipeline performance.
3. An increase in soil stiffness (shear wave velocity) generally increased the strain of the pipeline at the crest of the slope. This could be due to the decrease in displacement between the pipeline and the surrounding medium. For pipelines running along a slope, the critical maximum strain value on the pipeline was at the crest.
4. The bends in a pipeline crossing the slope crest strongly increased the amplification of the axial strain of the pipeline compared to that at the toe of the slope.
5. The amplification of input motion and strain on a pipeline at the crest was dependent on the natural frequency of the slope. When the significant frequency of the input motion approached the natural frequency of the slope, the amplification of input motion and strain on the pipeline increased.

Abbreviations
SF: Shape factor; 2D: Two-dimensional; 3D: Three-dimensional; D: Diameter; t: Thickness; D/t: Diameter-to-thickness ratio

Authors' contributions
MB and JE were responsible for the conceptualization, writing, interpretation and numerical analysis. MB, Mk and MD participated in quality control. All authors read and approved the final manuscript.

Availability of data and materials
The datasets used and/or analyzed in this study are available from the corresponding author upon reasonable request.

Declarations

Competing interests
The authors declare that they have no competing interests.

Author details
[1]Science and Research Branch, Islamic Azad University, Tehran, Iran. [2]International Institute of Earthquake Engineering and Seismology, Tehran, Iran.

References
ABAQUS 2012 ABAQUS user's manual version 6.12. Simulia
American lifelines alliance (ALA) (2001) Guidelines for the design of buried steel pipe (with addenda through 2005). American Society of Civil Engineers
American Petroleum Institute Specification for pipeline (2000) API specification 5L. Edition, Forty-Second
Assimari D, Jeong S (2013) Ground-Motion Observations at Hotel Montana during the M 7.0 2010 Haiti earthquake: topography or soil amplification? Bull Seismol Soc Am 103(5):2577–2590
Athanasopoulos GA, Pelekis PC, Leonidou EA (1999) Effects of surface topography on seismic ground response in the Egion, (Greece) 15 June 1995 earthquake. Soil Dyn Earthq Eng 18(135–149):2. https://doi.org/10.1016/S0267-7261 (98)00041-4
Behnamfar F, Saberi M, Vafaeian M (2013) A semi-analytical model for estimating seismic behavior of buried steel pipes at bend point under propagating waves. Bull Earthq Eng 11:1373–1402
Boore DM, Harmsen SC, Harding ST (1981) Wave scattering from a step change in surface topography. Bull Seismol Soc Am 71(1):117–125
BS EN 1998–5: 2004 Eurocode 8. Design of structures for earthquake resistance - Part 5. Foundations, retaining structures and geotechnical aspects
Buech F, Davies TR, Pettina JR (2010) The little red hill seismic experimental study: topographic effects on ground motion at a bedrock dominated mountain edifice. Bull Seismol Soc Am 100(5):2219–2229. https://doi.org/10.1785/012 0090345
Caserta A, Bellucci F, Cultrera G, Donati S, Marra F, Mele G, Palombo B, Rovelli A (2000) Study of site effects in the area of Nocera Umbra (Central Italy) during the 1997 Umbria-Marche seismic sequence. J Seismol 4(555–565):4. https:// doi.org/10.1023/A:1026510300469
Chavez-Garcia F, Sanchez LR, Hatzfeld D (1996) Topographic site effects and HVSR. A comparison between observation and theory. Bull Seismol Soc Am 86(5):1559–1573
Code 600 (2012) Loading and Seismic Analysis Guideline of Iran's Lifeline
Courant R, Friedrichs KO, Lewy H (1928) Über die partiellen differenzialgleichungen der mathematischen. Physik Math Ann 100: 32–74. doi: https://doi.org/10.1007/BF01448839, 1
Datta T (1999) Seismic response of buried pipelines: a state- of- the art review. Nuc Eng Design 192(2):271–284. https://doi.org/10.1016/S0029-5493 (99)00113-2
Davis LL, West LR (1973) Observed effects of topography on ground motion. Bull Seismol Soc Am 63:283–298
Duhee P, Se-Woong W, Sang-Jin K (2020) Estimation of seismically induced longitudinal strain in pipelines subjected to incident shear wave. KSCE J Civil Eng 24(8):2322–2332
GB50011 (2010) Code for seismic design of buildings, National Standard of people's republic of china
Geli L, Bard P-V, Julien B (1988) The effect of topography on earthquake ground motion: a review and new results. Bull Seismol Soc Am 78(1):42–63
Graizer V (2009) Low-velocity zone and topography as a source of site amplification effect on Tarzana hill, California. Soil Dyn Earthq Eng 29:324–332
Griffiths DW, Bollinger GA (1979) The effect of Appalachian Mountain topography on seismic waves. Bull Seismol Soc Am 69:1081–1105
Hailemikael S, Lenti L, Martino S, Paciello A, Rossi D, Mugnozza G (2016) Ground-motion amplification at the Colle di Roio ridge, Central Italy: a combined

effect of stratigraphy and topography. Geophy J Int 206(1):1–18. https://doi.org/10.1093/gji/ggw120

Hancox GT, Cox SC, Turnbull IM, Crozier MJ (2003) Reconnaissance studies of landslides and other ground damage caused by the Mw 7.2 Fiordland earthquake of 22 August 2003. Institute of Geological and Nuclear Sciences Science Report 2003/30, Lower Hutt

Hartzell SH, Carver DL, King KW (1994) Initial investigation of site and topographic effects at Robinwood ridge, California. Bull Seismol Soc Am 84:1336–1349

Isoyama R, Ishida E, Yune K, Shirouzo T (2000) Seismic damage estimation procedure for water supply systems. 12WCEE: Auckland, 4 2000

Jafarzadeh F, Shahrabi M, Jahromi HF (2015) On the role of topographic amplification in seismic slope instabilities. J Rock Mech Geotech Eng 1:1–8

Khan S, van der Meijde M, van der Werff H, Shafique M (2020) The impact of topography on seismic amplification during the 2005 Kashmir earthquake. Nat Hazards Earth Sys Sci 20(399–411):2. https://doi.org/10.5194/nhess-20-399-2020

Khazai B, Sitar N (2003) Evaluation of factors controlling earthquake-induced landslides, caused by chi-chi earthquake and comparison with the Northridge and Loma Prieta, events. Eng Geol 71:79–95

Kimiyasu O, Tatsuo O (2004) Damage Estimation of Supply Pipeline Damage Estimation of the water supply pipelines in artificially altered ground. 13th World Conference on Earthquake Engineering: Vancouver. August 1–6, 2004.

Kouretzis GP, Bouckovalas GD, Gantes CJ (2006) 3-d shell analysis of cylindrical underground structures under seismic shear (s) wave action. Soil Dyn Earthq Eng 26(10):909–921. https://doi.org/10.1016/j.soildyn.2006.02.002

Kuchleme RL, Lysmer J (1973) Finite element method accuracy for wave propagation problems. J Soil Mech Found Eng Div 99:421–428

LeBrun B, Hatzfeld D, Bard PY, Bouchon M (1999) Experimental study of the ground motion on a large scale topographic hill al Kitherion (Greece). J Seismol 3(1–15):1. https://doi.org/10.1023/A:1009745016671

Li H, Liu Y, Liu L, Liu B, Xia X (2019) Numerical evaluation of topographic effects on seismic response of single-faced rock slopes. Bull Eng Geol Environ 78:1873–1891, 3, doi: https://doi.org/10.1007/s10064-017-1200-7

Liu AI, Hu YX, Zhao FX, Li XJ, Takada S, Zhao L (2004a) An equivalent-boundary method for the shell analysis of buried pipelines under fault movement. Acta Seismol Sinica 17(150–156):S1. https://doi.org/10.1007/s11589-004-0078-1

Liu AW, Takada S, Hu Y-X (2004b) Shell model with an equivalent boundary for buried pipelines under the fault movement. 13th World Conference on Earthquake Engineering: Vancouver, August 1–6, 2004

Lovati S, Bakavoli MKH, Massa M, Ferretti G, Pacor F, Paolucci R, Haghshenas E, Kamalian M (2011) Estimation of topographical effects at Narni ridge (Central Italy): comparisons between experimental results and numerical modelling. Bull Earthq Engin 9(6):1987–2005. https://doi.org/10.1007/s10518-011-9315-x

Marzorati S, Ladina C, Falcucci E, Gori S, Ameri G, Galadini F (2011) Site effects "on the rock": the case of Castelvecchio Subequo (L'Aquila, Cnntral Italy). Bull Earthq Eng 9(3):841–868. https://doi.org/10.1007/s10518-011-9263-5

Massa M, Barani S, Lovati S (2014) Overview of topographic effects based on experimental observations: meaning, causes and possible interpretations. Geophys J Int 197(3):1537–1550. https://doi.org/10.1093/gji/ggt341

Massa M, Lovati S, D'Alema E, Ferretti G, Bakavoli M (2010) An experimental approach for estimating seismic amplification effects at the top of a ridge, and the implication for ground-motion predictions: the case of Narni (Central Italy). Bull Seismol Soc Am 100(3020–3034):6. https://doi.org/10.1785/0120090382

Mayoral JM, De la Rosa D, Tepalcapa S (2019) Topographic effects during the September 19, 2017 Mexico City earthquake. Soil Dyn Earthq Eng 125(3). https://doi.org/10.1016/j.soildyn.2019.105732

Meslem A, Yamazaki F, Maruyama Y, D'Ayala D, Naili M and Benouar D (2012) Effect of Topographic Reliefs on Building Damage Distribution in Boumerdes City during the 2003 Algeria Earthquake, 15th World Conference on. Earthquake Engineering, Lisbon.

Mitani Y, Wang F, Okeke AC, Qi W (2012) Dynamic analysis of earthquake amplification effect of slopes in different topographic and geological conditions by using ABAQUS. Progress Geo-Disast Mitigation Technol Asia: 469–490

Nakileza BR, Nedala S (2020) Topographic influence on landslides characteristics and implication for risk management in upper Manafwa catchment. Mt Elgon Uganda. Geoinviron Disast 7(27):1. https://doi.org/10.1186/s40677-020-00160-0

Nguyen K-V, Gatmiri B (2007) Evaluation of seismic ground motion induced by topographic irregularity. Soil Dyn Earthq Eng 27(183–188):2. https://doi.org/10.1016/j.soildyn.2006.06.005

O'Rourke T, Toprak S (1997) GIS assessment of water supply damage from the Northridge, earthquake. Workshop on earthquake engineering frontiers in transportation facilities. United States, New York

Oskouei AV, Ghaznavi A (2017) The effect of P-wave propagation on the seismic behavior of steel pipelines. Periodica Polytechnica Civil Eng 61(4):889–903

Pacific Earthquake Engineering Research Center, n.d., https://peer.berkeley.edu/, PEER

Paolucci R (2002) Amplification of earthquake ground motion by steep topographic irregularities. Earthq Eng Struct Dyn 31(1831–1853):10. https://doi.org/10.1002/eqe.192

Pedersen H, Le Brun B, Hatzfeld D, Campillo M, Bard PY (1994) Ground-motion amplitude across ridges. Bull Seismol Soc Am 84:1786–1800

Prodromos NP (2012) Designing pipelines in areas with moderate or high seismic risk: geohazard assessment beyond EC8 provisions, 7th pipeline technology conference: Hannover, 28–30 Mar 2012

Qi WH (2011) FEM seismic analysis on the effect of topography and slope structure for landsliding potential evaluation. Master thesis for National Graduate Institute for policy studies, Tsukuba

Rahimi N, Arzani H, Mahmoudi M (2019) Evaluating the effects of earthquake wave propagation on buried curved pipes using static analysis. Int J Civil Eng 17(1353–1361):9. https://doi.org/10.1007/s40999-019-00410-9

Rizzitano S, Cascone E, Biondi G (2014) Coupling of topographic and stratigraphic effects on seismic response of slopes through 2D linear and equivalent linear analyses. Soil Dyn Earthq Eng 67:66–84. https://doi.org/10.1016/j.soildyn.2014.09.003

Saberi M, Arabzadeh A, Keshavarz A (2011) Numerical analysis of buried pipelines with right angle elbow under wave propagation. Proced Eng 14:3260–3267. https://doi.org/10.1016/j.proeng.2011.07.412

Saberi M, Behnamfar F, Vafaeian M (2015) A continuum Shell-beam finite element modeling of buried pipes with 90-degree elbow subjected to earthquake excitations. Int J Eng 28(3):338–349

Sepúlveda SA, Murphy W, Jibson RW, Petley DN (2005a) Seismically induced rock slope failures resulting from topographic amplification of strong ground motions: the case of Pacoima canyon, California. Eng Geol 80: 336–348, 3-4, doi: https://doi.org/10.1016/j.enggeo.2005.07.004

Sepúlveda SA, Murphy W, Petley DN (2005b) Topographic controls on seismic rock slides during the 1999 chi-chi earthquake. Taiwan. Quart J Eng Geol Hydrogeol 38(189–196):2. https://doi.org/10.1144/1470-9236/04-062

Shabani MJ, Ghanbar A (2020) Design curves for estimation of amplification factor in the slope topography considering nonlinear behavior of soil. Indian Geotech J 50(907–924):6. https://doi.org/10.1007/s40098-020-00443-1

Spudich P, Hellweg M, Lee WHK (1996) Directional topographic site response at Tarzana observed in aftershocks of the 1994 Northridge, California, earthquake: implications for main shock motions. Bull Seismol Soc Am 86(1):193–208

Takada S, Hassani N, Fukuda K (2001) A new proposal for simplified design of buried steel pipes crossing active faults. Earthq Eng Struct Dyn 30(8):1243–1257. https://doi.org/10.1002/eqe.62

Takada S, Higashi S (1992) Seismic response analysis for jointed buried pipeline by using shell fem model. Proceedings of the tenth world conference on earthquake engineering 5487-5492

The Iranian Code of Practice for Seismic Resistant Design of Buildings (Standard 2800) 2015 4th edition

Tromans I (2004) Behavior of buried water supply pipelines in earthquake zones. PHD Thesis, Imperial College of Science, Technology and Medicine

Wolf JP (1985) Dynamic soil-structure interaction, Prentice Hall Int.

Yimsiri S, Soga K, Yoshizaki K, Dasari G, O'Rourke T (2004) Lateral and upward soil-pipeline interactions in sand for deep embedment conditions. J Geotech Geoenviron Eng 130(8):830–842. https://doi.org/10.1061/(ASCE)1090-0241(2004)130:8(830)

Publisher's Note